

Chaotic Billiards

Hans Jürgen Korsch and Frank Zimmer

Fachbereich Physik, Univ. Kaiserslautern, D-67653 Kaiserslautern, Germany

Abstract. The frictionless motion of a particle on a plane billiard table bounded by a closed curve provides a very simple example of a conservative classical system with non-trivial, chaotic dynamics. The limiting cases of strictly regular (“integrable”) and strictly irregular (“ergodic”) systems can be illustrated, as well as the typical case which shows an intricate mixture of regular and irregular behavior. Irregular orbits are characterized by an extremely sensitivity with respect to the initial conditions. Such billiard systems are exemplarily suited for educational purposes as models for simple systems with complicated dynamics as well as for far-reaching fundamental investigations.

1 Introduction

In the past decades, classical physics has witnessed an unexpected, impetuous development, which has led to an entirely new understanding of the classical dynamics of simple systems, an area in physics that has usually been presumed to be generally understood and concluded. It became evident, however, that – contrary to the concepts conveyed by most physics textbooks – even simplest, completely deterministic systems may show irregular, chaotic behavior, that is as unpredictable as the tossing of a coin. Commonly one accepted a random, stochastic behavior only for a system with a large ($\approx 10^{23}$) number of degrees of freedom, e.g., a gas. It has now been established that such a behavior can be exhibited by systems with merely *two* degrees of freedom, hence a very small number. The motion of a particle in a two-dimensional conservative force field, i.e. in a potential, *typically* shows chaotic behavior. Since the first indication of chaos in strictly deterministic systems, a torrent of scientific studies has set in, in which the existence of such a “deterministic chaos” has been analyzed and further verified.

Chaotic systems in physics can be divided into two groups: There are so-called dissipative systems, where friction is present, and then conservative systems, where energy is a constant of motion. We shall exclusively deal with the latter case here. As an introduction to the discussed dynamics of conservative systems, the textbooks by Lichtenberg and Liebermann [1] and Schuster [2] as well as the excellent review article by Berry [3] are recommended.

The description of a system with N degrees of freedom necessitates, as we know, $2N$ coordinates, namely N position coordinates $q = (q_1, q_2, \dots, q_N)$ and N canonical momenta $p = (p_1, p_2, \dots, p_N)$. The time-evolution of the system is

therefore given by $(q(t), p(t))$, a curve in a $2N$ -dimensional space, the so-called phase space.

This curve is determined by the Hamiltonian differential equations of motion

$$\dot{p}_i = -\frac{\partial H}{\partial q_i}, \quad \dot{q}_i = \frac{\partial H}{\partial p_i}, \quad i = 1, \dots, N. \quad (1)$$

The textbooks in classical mechanics, with some rare exceptions, deal with so-called *integrable* systems, i.e. there exist N independent constants of motion F_j , $j = 1, \dots, N$, which are functions on phase space whose values do not change along the trajectory. In addition, one must demand that these functions $F_j(q, p)$ are “in involution”, i.e. their Poisson brackets vanish:

$$\{F_j, F_k\} = \sum_i \left(\frac{\partial F_j}{\partial p_i} \frac{\partial F_k}{\partial q_i} - \frac{\partial F_k}{\partial p_i} \frac{\partial F_j}{\partial q_i} \right) = 0. \quad (2)$$

Because of the N conditions $F_j(q, p) = f_j = \text{const.}$, the motion is restricted to an N -dimensional manifold in $2N$ -dimensional phase space whose topology is that of an N -torus [3–5]. Moreover, this must be true for *any* trajectory and therefore the phase space is densely filled with such nested tori. Such a dynamics is called regular.

In a so-called conservative Hamiltonian system, the energy is one of the constants of motion and consequently a one-dimensional conservative system is always integrable. In the following we shall discuss the simplest non-trivial case, namely two-dimensional conservative systems, which are thus integrable if there exists yet another independent conserved quantity F , i.e. with $\{H, F\} = 0$. Integrable systems are, opposed to common belief, extremely rare. The probability for the integrability of a randomly chosen system with more than one degree of freedom is equal to zero. Integrability can, however, often be related to symmetry: the motion of a particle in a *central* force field belongs to the few examples of integrable systems. The opposite of an integrable system is an *ergodic* system, for which almost every orbit fills the available (for this energy!) phase space densely. Such an orbit is called *irregular* or *chaotic*. There exist only few systems for which ergodicity has been rigorously proven. One of these systems is the stadium billiard, i.e. a rectangle with semi-circular ends [6]. The typical case is a system which is neither fully regular nor chaotic and contains both regular and irregular orbits. Well-known examples are the double pendulum and the three-body problem of celestial mechanics.

In order to visualize the complicated dynamics and to simplify its handling, one uses a reduction of information by introducing a surface of section in phase space: instead of studying the entire orbit, one keeps track only of the sequence (q_n, p_n) , $n = 0, 1, 2, \dots$ of its intersection points with this surface of section. In this manner we obtain a discrete mapping

$$(q_n, p_n) \xrightarrow{T} (q_{n+1}, p_{n+1}) \quad (3)$$

which associates each intersection point with its successor. For a Hamiltonian system such a *Poincaré* map T is area preserving. The set of all intersection

points is called the *Poincaré section* of the orbit. In such a section one can easily distinguish the different types of orbits.

Billiard systems are exemplarily suited as models for educational purposes (as well as for far-reaching fundamental investigations!) since the billiard motion is easy to comprehend and the numerical treatment does not, opposed to many other systems, require numerical integration of differential equations. This is an important advantage, since such a computation is, even by using modern computers, comparatively time-consuming, especially since chaotic phenomena are exhibited in the long-time behavior of an orbit. Furthermore, numerical methods for solving differential equations are not exact, and show instabilities, which can not always be clearly distinguished from the true chaotic behavior.

2 Billiard Systems

The two-dimensional billiard problem [6,7] describes a point particle moving without friction on a plane billiard table, bounded by a closed curve. Between the impacts at the boundary, the particle moves on straight lines with constant velocity. It is reflected at the boundary according to the reflection law: the angle of incidence is equal to the angle of reflection. We shall deal with convex billiards here, i.e. a straight line has at most two intersection points with the boundary curve, which reads in polar coordinates

$$r = r(\varphi). \quad (4)$$

For a sufficiently smooth boundary curve such billiards are non-ergodic [6,8].

In the billiard system, the Poincaré section evolves quite naturally from the boundary curve. This means that the intersection points are represented by the data at impact with the boundary, namely the angle φ at this point and the direction of the trajectory after the impact, which can be measured by the angle α with respect to the tangent (see Fig. 1). It is more convenient, however, to use

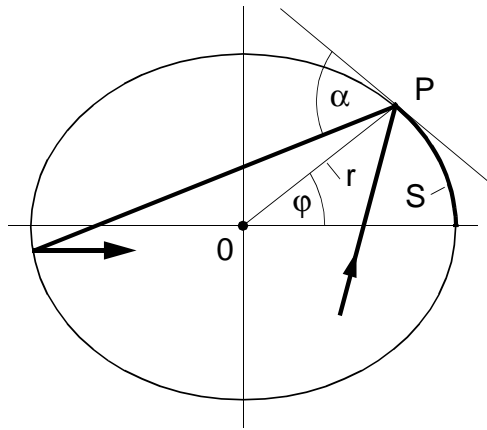


Fig. 1. Boundary curve $r(\varphi)$ of a billiard system, an initial part of a billiard trajectory and the coordinates: the arc length $S(\varphi)$ and $p = \cos \alpha$ ($\alpha =$ angle between trajectory and tangent of the boundary curve).

the projection on the tangent

$$p = \cos \alpha \quad (5)$$

and the arc length divided by the total length L of the boundary curve:

$$S(\varphi) = \frac{1}{L} \int_0^\varphi \sqrt{r^2(\varphi') + (dr/d\varphi')^2} d\varphi'. \quad (6)$$

The Poincaré map T relates the data of the n -th impact $P_n = (S_n, p_n)$ to the next one $P_{n+1} = (S_{n+1}, p_{n+1})$. This mapping can be shown to be area preserving using these variables:

$$\det \frac{\partial(S_{n+1}, p_{n+1})}{\partial(S_n, p_n)} = 1. \quad (7)$$

More details about this mapping are given in the appendix. Numerically the problem is quite simple: one has to compute the intersection of the trajectory (a straight line) with the boundary curve, which yields the next impact angle φ_{n+1} . Then the arc length S_{n+1} is evaluated from eq. (6) and the angle α_{n+1} between the trajectory and the tangent of the boundary curve at this point is determined, as well as $p_{n+1} = \cos \alpha_{n+1}$ and the reflected trajectory. Then this process is continued to obtain the next impact data.

2.1 The Billiard Computer Program

For a comfortable study of the billiard dynamics an interactive computer program BILLIARD was developed which allows efficient computations without any prior knowledge of computing. This program is contained in a collection of PC programs illustrating chaotic dynamics for a selection of systems with applications in physics [9]. In the billiard program some pre-set billiards can be chosen or an arbitrary boundary curve $r(\varphi)$ can be inserted via the keyboard. The program shows position and phase space presentations of an orbit for variable initial conditions. Comments concerning the numerical algorithm can be found in the appendix. In the following we describe some numerical experiments which are carried out using this program.

3 Integrable Systems

3.1 Circular Billiards

For a circular billiard $r(\varphi) = r_0$ the reflections of the orbit can be evaluated very easily. One finds the explicit equation

$$\varphi_n = \varphi_0 + 2\alpha n \quad (8)$$

for the angle of the n -th impact. The direction angle α or the projection $p = \cos \alpha$ on the tangent direction is constant along the orbit which constitutes conservation of angular momentum L . We have a second constant of motion, L , and the

circular billiard is therefore integrable. In phase space each orbit lies on a two-dimensional surface, whose intersection with the (S, p) -plane is a curve. Since the coordinate p represents a conserved quantity, these invariant curves appear as horizontal lines. For orbits with a rational angle ratio

$$\alpha_n = \frac{m}{k} \pi, \quad m, k \in \mathbb{N} \quad m < k, \tag{9}$$

we have

$$\varphi_n = \varphi_0 + \frac{m}{k} 2\pi n, \tag{10}$$

i.e. the orbits are periodic and close after k cycles. Such an orbit is called k -periodic. In such a case, the Poincaré section consists of a series of k discrete points (S_n, p_n) , $n = 1, \dots, k$, which are traversed periodically:

$$T^k(S_n, p_n) = (S_n, p_n). \tag{11}$$

For this reason the k points (S_n, p_n) are called *fixed points* of the mapping

$$T^k = \underbrace{T \circ T \circ \dots \circ T}_{k \text{ -times}}. \tag{12}$$

For angles that are *not* rational multiples of π , the iterated points (S_n, p_n) fill, with growing n , a horizontal line densely, a so-called *invariant curve*, because it is invariant under the Poincaré map T . Figure 2 shows such an irrational orbit; radial distances $< p$ are forbidden due to conservation of angular momentum.

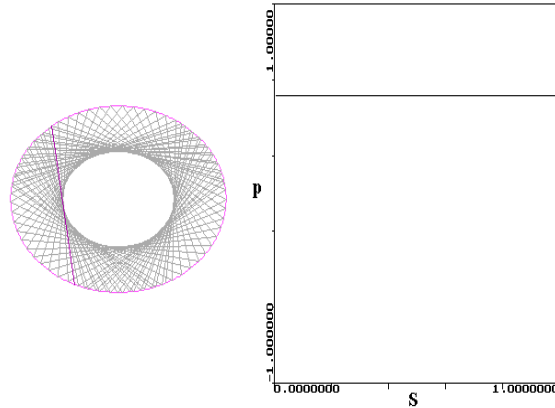


Fig. 2. Circular billiard. A non-periodic orbit in position space (left) appears as a straight line in the phase space diagram (S, p) (right).

The motion along the orbit can be divided into two components: an oscillation between the inner envelope and the outer boundary curve and a rotation about

the center. For a k -periodic orbit with $\alpha = m\pi/k$ the frequencies related to these partial motions have the ratio

$$\frac{\omega_1}{\omega_2} = \frac{m}{k}, \quad (13)$$

i.e. for $\pi/5$ we find five oscillations between the inner and outer boundary curve and a single rotation of 2π ; for $2\pi/5$ we have two such rotations.

3.2 Elliptical Billiards

We shall now consider an elliptical billiard with eccentricity ϵ , i.e. the boundary curve is given by

$$r(\varphi) = \frac{b}{\sqrt{1 - \epsilon^2 \cos^2 \varphi}} \quad (14)$$

with semi-minor axis b and semi-major axis $a = b(1 - \epsilon^2)^{-1/2}$. Figure 3 depicts such an ellipse with $\epsilon = 0.3$. For large values of p , the orbits are similar to those for a circular billiard. Such an orbit fills an annular area in position space and possesses an enveloping curve, that separates a forbidden inner region. It can be shown that this enveloping curve – called caustic – is again an ellipse with the same foci as the boundary ellipse. The orbit always intersects the large diameter of the ellipse outside the line connecting both foci. For small values of p a different type of motion appears: the position space orbit fills an area which is bounded by two con-focal hyperbolic curves.

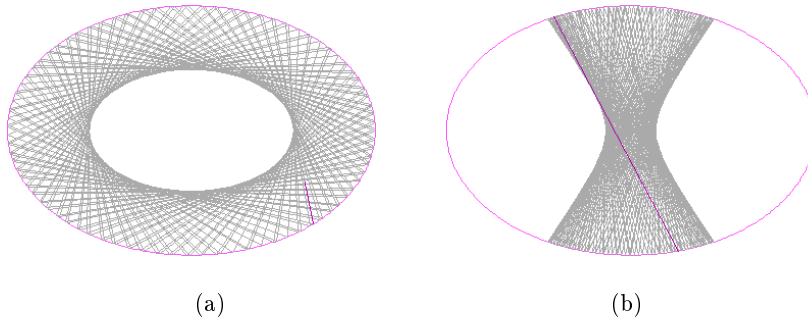


Fig. 3. Elliptical billiard (eccentricity $\epsilon = 0.3$). Orbits which intersect the main axis in the sections outside the two foci are bounded by an elliptical envelope (a); orbits passing between the two foci have a hyperbolic envelope (b).

Figure 4 shows a Poincaré section in the (S, p) -plane for a number of trajectories with different initial conditions. Two different kinds of orbits, as described above, can be distinguished (compare also Fig. 3). For large p , the iterated phase space points trace out a more or less undulating curve. For small values of p , the phase space points alternate between two islands. When iterated, the orbit

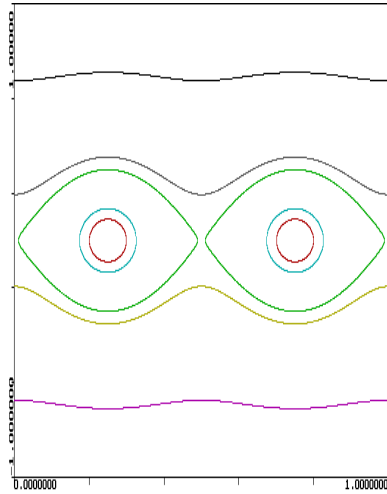


Fig. 4. Elliptical billiard (eccentricity $\epsilon = 0.3$). Shown is a Poincaré section in the (S, p) -plane. Different types of orbits can be distinguished (compare Fig. 3).

fills two disconnected closed curves. The two types of motion are separated in phase space by a separation curve (a *separatrix*), that approximately satisfies the equation

$$p(S) \approx \pm \epsilon \sin(2\pi S) \quad (15)$$

(see below). In the center of the separatrix we find a 2-periodic orbit along the minor axis (with length $l = 2b$) expressed in other terms: the mapping T^2 possesses a fixed point there. This orbit is stable, i.e. sufficiently close orbits always remain in its neighborhood [6]. This numerically observed stability can also be verified analytically using Eqs. (38) and (41) in the appendix, which yield for the stability matrix of the diametrical two-bounce orbit

$$\mathbf{M}_2 = \begin{pmatrix} 2 \left(\frac{l}{\rho} - 1 \right)^2 - 1 & 2l \left(1 - \frac{l}{\rho} \right) \\ \frac{2}{\rho} \left(\frac{l}{\rho} - 1 \right) \left(2 - \frac{l}{\rho} \right) & 2 \left(\frac{l}{\rho} - 1 \right)^2 - 1 \end{pmatrix}, \quad (16)$$

where ρ is the radius of curvature at the points of impact. The stability condition $|\text{Tr}\mathbf{M}_2| < 2$ (see Eq. (43)) is in this case simply

$$l < 2\rho, \quad (17)$$

which immediately implies stability of the orbit along the minor axis ($l = 2b < 2\rho$) and instability of the orbit along the mayor axis (here we have $l = 2a > 2\rho$)¹.

Orbits on the separatrix pass through both foci. These orbits clearly demonstrate the focal properties of an ellipse. The separatrix orbit with $p = 0$ is a 2-periodic orbit along the large diameter, which is, in contrast to the small

¹ From eq. (39) we easily deduce $\rho = a^2/b$ for the minor-axis orbit and $\rho = b^2/a$ for the major axis.

diameter orbit, unstable, which means that even smallest deviations from the initial values yield orbits that do not remain in its vicinity. As with the circle, the impact positions of an orbit either constitute fixed points of the Poincaré presentation (rational circular frequency), which implies a periodic orbit, or the impact positions fill a curve densely. In this case we have an irrational circular frequency and the orbit fills densely a two-dimensional surface in phase space, whose section is then an invariant curve in Fig. 4. Since this holds true for all orbits – invariant curves fill the phase space section completely – the elliptical billiard and the circular billiard represent integrable systems. Aside from the energy, there exists yet another conserved quantity, F . A simple consideration [7,9] shows, that the product of the angular momenta with respect to the two foci remains unchanged in a collision with an elliptical boundary. After an elementary calculation described in the appendix, one obtains for the invariant

$$F(\varphi, \alpha) = \frac{1}{2} \left\{ r^2 - \epsilon^2 a^2 + (a^2 - \epsilon^2 r^2 \cos^2 \varphi) \cos(2\alpha) \right\}. \quad (18)$$

Minima of F lie at $\varphi = \pi/2$ or $3\pi/2$ with $\alpha = \pi/2$, where F has the value $-\epsilon^2 a^2$. On the separatrix we have $F = 0$ (the orbit passes through both foci). For small values of ϵ one obtains the expression (15) for the separatrix. The circular billiard and its constant of motion, the angular momentum L , appears as a special case of the elliptical billiard.

4 “Typical” Billiards

The elliptical billiard is the *only* convex billiard with a smooth boundary curve that leads to integrable dynamics. This conjecture by Poritsky (1950) [10] has been proven in 1991 by Amiran (see [11], page 120). It is therefore a very atypical system. As an example of a “typical” billiard we shall in the following study the boundary curve

$$r(\varphi) = 1 + \epsilon \cos \varphi \quad (19)$$

(a similar one has been investigated by Robnik [8]). With increasing deformation ϵ this curve deforms from a circle, for $\epsilon = 0$, into a cardioid-like curve for $\epsilon = 1$. In the region between $0 \leq \epsilon \leq 0.5$ the boundary curve is convex. We shall limit ourselves to this case in the following discussion. Phase space presentations for $\epsilon = 0.1$ to $\epsilon = 0.5$ are displayed in figures 5(a) to (d) and 6. One encounters a qualitatively different behavior compared to the elliptical billiard. The differences become more distinct with growing ϵ . For small deformations $\epsilon = 0.1$ or $\epsilon = 0.2$ the picture structurally resembles closely that of an elliptical deformation of the circle-billiard: the 2-periodic orbits for $p = 0$ are broken apart into a stable and an unstable orbit, which bounce back and forth between $(S, p) = (0, 0)$ and $(1/2, 0)$ or $(1/4, 0)$ and $(3/4, 0)$, respectively. One should note, however, that for the curve (19) the diameter of the billiard in the horizontal direction is independent of ϵ , while the diameter in the vertical direction increases with ϵ . For small values of ϵ , we find a maximum of the diameter at $\cos \varphi \approx \epsilon$ with

magnitude $a \approx 1 + \epsilon^2/2$. An ellipse with the same diameters therefore has an eccentricity $(1 - (b/a)^2)^{1/2} \approx \epsilon$. If one approximates the billiard by an ellipse, the latter appears to be turned by 90° compared to the one studied in section 3. Apart from this, the basic structures of the phase space diagrams for $\epsilon = 0.2$, for example, are very similar (compare Fig. 5(b) and Fig. 4).

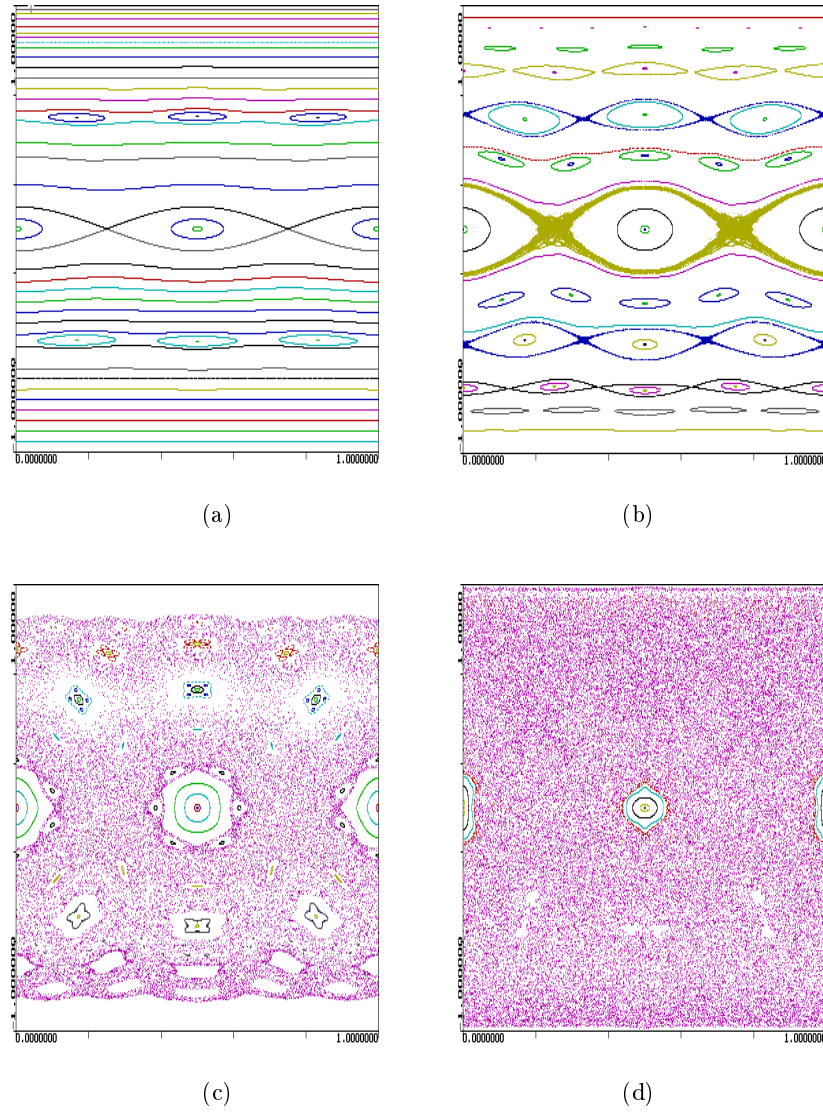


Fig. 5. Phase space diagram (S, p) for the typical billiard (19) for various values of the deformation parameter: $\epsilon = 0.1$ (a), 0.2 (b), 0.3 (c), 0.4 and (d).

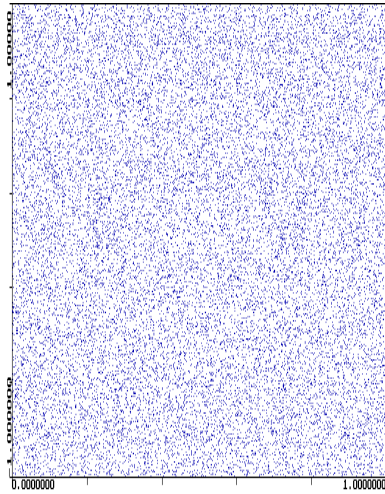


Fig. 6. Phase space diagram (S, p) for the typical billiard (19) for a deformation parameter $\epsilon = 0.5$.

The resemblance with an elliptical billiard for small values of ϵ is merely superficial. Even for $\epsilon = 0.1$ some clear island chain structures can be discerned, a first indication for the non-integrability of our billiard. If one studies the island structures more closely, one finds in the center of these islands an n -periodic orbit, for example the 3-periodic orbit in Fig. 5(a) for $\alpha = \pi/3$, ($p = \cos \alpha \approx 0.5$), the 4-periodic orbit for $\alpha \approx \pi/4$ ($p \approx 0.707$) or both 5-periodic orbits at $\alpha \approx \pi/5$ ($p \approx 0.809$) and $\alpha \approx 2\pi/5$ ($p \approx 0.309$). The centers of the island chains in Fig. 5(a) consist of stable fixed points of T^n for $n = 2, 3, \dots$. Between these stable fixed points one finds unstable fixed points of T^n . This appears to be quite similar to the metamorphosis of the 2-periodic orbits in the transition circle \rightarrow ellipse (figure 4). The second major difference to the phase space presentation of the ellipse is the appearance of *irregular* orbits. One can recognize orbits in the vicinity of the unstable fixed points, whose Poincaré sections no longer trace out a curve but fill an *area* in phase space. This necessitates the non-existence of a constant of motion, and it is therefore quite astonishing that the majority of orbits behaves as though one existed. Most orbits again fill, upon iteration, an invariant curve.

We shall formulate the behavior of our circle-billiard with a small perturbation in a somewhat different manner. The so-called KAM-theorem is important here, named after the mathematical physicists A. N. Kolmogorov, V. I. Arnold, and J. Moser, [1–4]. In the proof of this theorem, a sufficiently often differentiable potential is a pre-requisite, which is not fulfilled by our hard-bounded billiard. The statements of the KAM-theorem can therefore only be applied with some caution. The KAM-theorem states that for a perturbed integrable system those invariant curves remain unchanged, whose frequency ratio between radial and angular oscillation is sufficiently irrational. More precisely, all invariant orbits with

$$\left| \frac{\omega_1}{\omega_2} - \frac{m}{k} \right| > \frac{C(\epsilon)}{k^{5/2}} \quad (20)$$

for arbitrary coprime natural numbers m and k remain unchanged (with the assumption $\omega_1 < \omega_2$).

$C(\epsilon)$ is a constant depending on the perturbation ϵ of the integrable system and approaches 0 for $\epsilon = 0$. Around each rational frequency ratio $\omega_1/\omega_2 = m/k$ there exists a narrow region of the size $C(\epsilon)k^{-5/2}$, in which (20) is *not* satisfied. For a more irrational frequency ratio, i.e. a larger denominator k in m/k , the region excluded by (20) appears to be more narrow. Since the set of rational numbers ω_1/ω_2 is dense in the interval $[0, 1]$ and for every rational frequency ratio m/k an entire interval

$$\left| \frac{\omega_1}{\omega_2} - \frac{m}{k} \right| \leq \frac{C(\epsilon)}{k^{5/2}} \quad (21)$$

is excluded by (20), one could assume that (20) is practically never satisfied. This is, however, *not* the case. A simple estimate yields for the union of all intervals violating (20)

$$\sum_{m < k}' \left| \frac{\omega_1}{\omega_2} - \frac{m}{k} \right| < \sum_k \sum_{m=1}^k \left| \frac{\omega_1}{\omega_2} - \frac{m}{k} \right| \leq \sum_k k C(\epsilon) k^{-5/2} = C(\epsilon) \sum_k k^{-3/2} \quad (22)$$

where the primed sum denotes that m and k have no common integer divisor. Since the sum $\sum_k k^{-3/2}$ converges, the interval sum in (22) goes with ϵ to zero (as $C(\epsilon)$ does), i.e. for a sufficiently small perturbation ϵ the area which is *not* filled with invariant curves can be made arbitrarily small. The majority of invariant curves remains unchanged even in the perturbed system. A closer inspection of the phase space diagrams 5(a), 5(b) confirms these statements.

The invariant curves in the zones excluded by the KAM-condition are typically destroyed. Rational orbits with $\omega_1/\omega_2 = m/k$ decay into ℓk stable and ℓk unstable fixed points, where the natural number ℓ is often equal to one (compare the theorem of Poincaré and Birkhoff [3]). This is also confirmed by Figs. 5(a) and 5(b).

These statements are valid for small deformations ϵ . With increasing ϵ the destroyed zones grow, and the chaotic area-filling orbits in phase space increase. The “chaotic sea” is, at the beginning, still enclosed by intact invariant curves (compare Fig. 5(b)). With increasing ϵ a growing number of invariant curves is destroyed. For $\epsilon = 0.3$ we find an extended chaotic region. All points in this wide chaotic band $|p| \approx 0.77$ are created by a single orbit. Only small islands with invariant curves remain. For $\epsilon = 0.4$ these regions are further diminished and for $\epsilon = 0.5$ we find only very small visible islands (for example at $\alpha = 90^\circ$, $\varphi = 143.13^\circ$). All points in Fig. 6 originate from a single orbit.

5 Further computer experiments

5.1 Uncertainty and Predictability

In the previous section we have seen that regular and irregular or “chaotic” orbits can be distinguished by their phase space behavior. There exists yet another

characteristic of chaotic orbits: in the regular case, initially neighboring orbits remain quite close. For irregular, chaotic orbits this does not hold true and trajectories separate extremely fast. Here very important questions arise concerning the long-time predictability of strictly deterministic processes.

For the simple case of a circular billiard the effects of an initial uncertainty ($\delta\varphi_0, \delta\alpha_0$) can easily be derived. We find

$$\delta\varphi_n = \delta\varphi_0 + 2\delta\alpha_0 n, \quad (23)$$

i.e. the errors grow linearly. Similar relations are valid for other integrable cases and for regular orbits in general. The irregular case is completely different: here the orbits are very sensitive to small deviations in the initial conditions and the initial uncertainties grow *exponentially*:

$$|\delta\varphi_n| = |\delta\varphi_0| e^{\lambda n}, \quad (24)$$

where the coefficient λ is known as the *Lyapunov Exponent*.

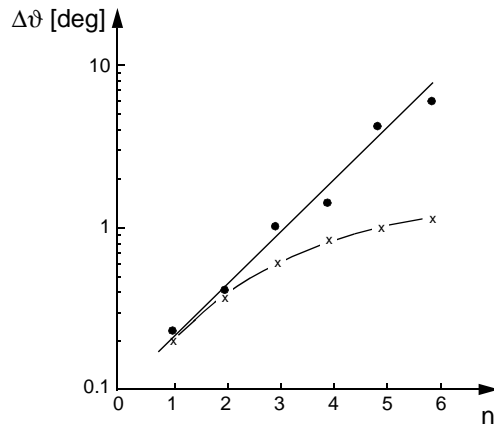


Fig. 7. Angle difference $\delta\varphi_n$ of two initially close orbits as a function of the number of impacts n for a chaotic orbit (\bullet) of the billiard (15) with $\epsilon = 0.5$ and for a regular orbit (\times) of the circle-billiard.

Figure 7 shows the angular separation for two orbits of the chaotic billiards (19) for $\epsilon = 0.5$ with $\varphi_0 = 0$ and $\alpha_0 = 70^\circ$ and 70.1° as a function of n on a logarithmic scale. The exponential law (24) is approximately satisfied with $\lambda = 0.7$. For comparison, the separation of two regular orbits of a circular billiard is also plotted, where the errors grow linearly.

The consequences of the depicted behavior: An orbit is completely unpredictable if, for example, the angular precision reaches the value $\delta\varphi_{\max} = 2\pi$. Under the conditions of Fig. 7 the destiny of the regular orbit is predictable up to about 1800 impacts with the boundary, in the irregular case merely

$$n_{\max} = \frac{1}{\lambda} \ln \frac{\delta\varphi_{\max}}{\delta\varphi_0} \approx \frac{1}{0.7} \ln \frac{360}{0.1} \approx 12. \quad (25)$$

Doubling the initial precision doubles the predictability of the regular case to 3600 impacts, in the irregular case it only increases by $(\ln 2)/\lambda$ to $n_{\max} \approx 12 +$

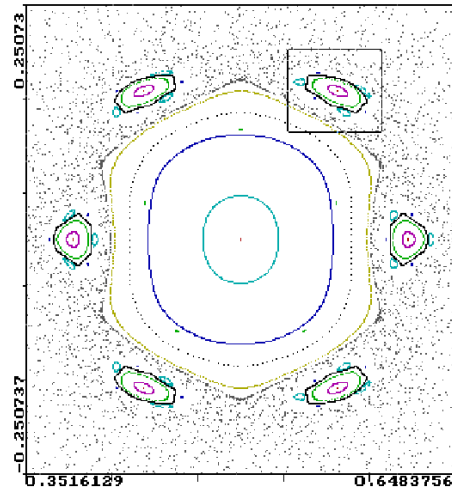


Fig. 8. Magnification of the neighborhood of the central fixed point in Fig. 5(c).

$(\ln 2)/0.7 \approx 13$. This exponential increase in the uncertainty and the merely logarithmic increase of the predictability is characteristic of chaotic orbits. A predictability of about 100 impacts with the conditions of Fig. 7 yields a required initial precision of the angle to be $2\pi e^{-70} \approx 2 \cdot 10^{-30}$. It is therefore impossible, or only possible with an unrealistic effort, to make long term predictions even for strictly deterministic dynamics.

5.2 Fine Structure in Phase Space

The last example showing the complexity of non-integrable dynamics draws our attention to the fine structure of the phase space. We have seen that invariant curves with a rational frequency ratio break up into chains of stable and unstable fixed points. Now each of these stable fixed points is itself a center of a system of invariant curves, which can be broken apart even further. Figure 8 shows a

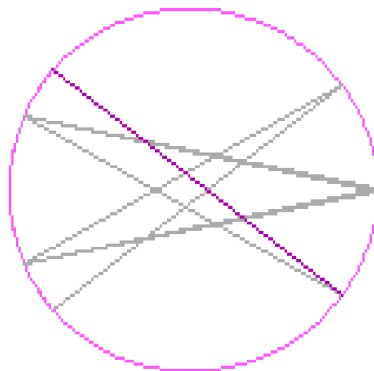


Fig. 9. Periodic orbit in the center of the six islands of Fig. 8.

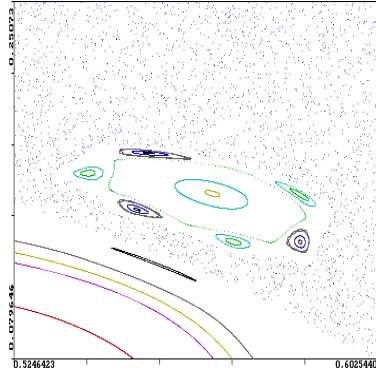


Fig. 10. Magnification of the island in the upper right corner of Fig. 8.

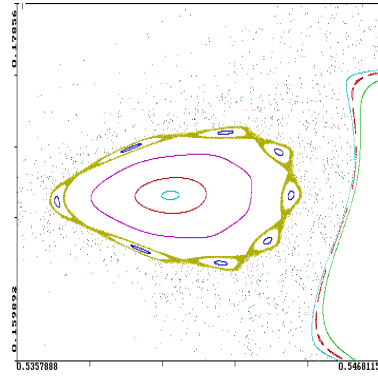


Fig. 11. Magnification of the island in the upper left corner of Fig. 10.

magnification of the vicinity of the central 2-periodic fixed point of Fig. 5(c). The neighborhood of this fixed point shows a system of invariant curves with narrow, broken-up rational orbits. This becomes especially evident for the six outer islands: they belong to a periodic orbit with period 12 in the center of these islands. Figure 9 shows these orbits in position space. Magnifying once more, for example the island at the upper right corner of Fig. 8, one finds a similar island structure again, as displayed in Fig. 10. A stable fixed point of T^{12} is located in the center, which is again surrounded by a system of invariant curves and by regions broken apart into stable and unstable fixed points. Figure 11 shows a further magnification of an island in Fig. 10. In principle, we can continue this magnification into deepest depths. Each fixed point “is a microcosmos of the whole, down to arbitrarily small scales” (M. V. Berry [3]).

In the present study we can only give a glimpse of the myriad of fascinating phenomena of chaotic dynamics, which can be illustrated in a simple fashion by a billiard system. Much could not be mentioned here, as for example the metamorphosis of stable periodic orbits with increasing perturbation parameter by a sequence of period-doublings. We refer to the literature [1–4,6] where these and other phenomena are discussed.

6 Gravitational Billiards

Another class of frequently studied billiard systems are *gravitational billiards*, a mass point moving freely in a homogeneous gravitational field which is reflected elastically from a hard convex surface (in three space dimensions) or a hard convex boundary curve (in two space dimensions). Here we only consider the latter case. The most prominent example of such a system is the wedge billiard [12–15]. Figure 12 illustrates the motion in such a symmetric wedge, which consists of a

sequence of reflections at the boundary (two straight lines for the wedge billiard) connected by parabolic trajectories.

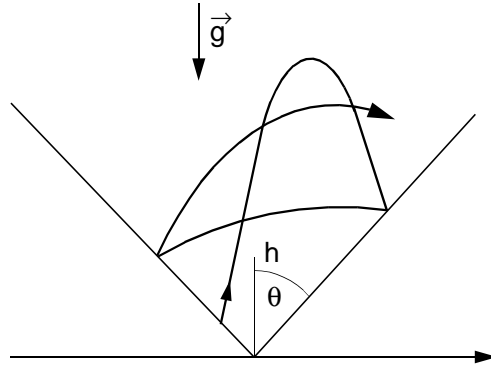


Fig. 12. Hopping of a mass point in a wedge under the action of a gravitational field.

The dynamics can be worked out analytically in this case, leading to a simple two-dimensional mapping, which can be most conveniently formulated in velocity space. Using the components v_x and v_y parallel or orthogonal to the wedge, respectively, — or even better —

$$X = v_x / \cos \theta, \quad Y = v_y / \sin \theta, \quad (26)$$

where θ is half of the opening angle of the wedge, one can derive a simple mapping equation

$$X_{n+1} = F(X_n, Y_n), \quad Y_{n+1} = G(X_n, Y_n), \quad (27)$$

where F and G are simple elementary functions (see [12–15] for details). Graphically, the iteration can be conveniently displayed in terms of the variables X_n and $Z_n = Y_n^2$, where the mapping

$$(X_n, Z_n) \longrightarrow (X_{n+1}, Z_{n+1}) \quad (28)$$

is again area preserving. These equations are used for the numerical iterations and the theoretical analysis. In the displayed velocity space sections, $x = v_x$ and $z = v_y^2$ are plotted. First of all, conservation of the energy

$$E = \frac{m}{2} (v_x^2 + v_y^2) + mgh. \quad (29)$$

where h is the height with respect to the vertex of the wedge, or — using scaled units —

$$1 = x^2 + z + h \quad (30)$$

restricts the dynamics in velocity space to the parabolic region

$$0 \leq z = 1 - x^2 - h \leq 1 - x^2. \quad (31)$$

Trajectories directly hitting the vertex ($h = 0$) map to the parabolic boundary $z = 1 - x^2$; the base line $z = 0$ describes a sliding motion along the wedge and points on the line $x = 0$ are trajectories orthogonal to the wedge. Contrary to the billiard systems discussed in the preceding sections, the dynamics of the wedge billiard depends on a single parameter, the wedge angle θ .

The program WEDGE — again chosen from the collection of programs for chaotic systems [15] — can be used to explore the interesting dynamical features of the wedge billiard.

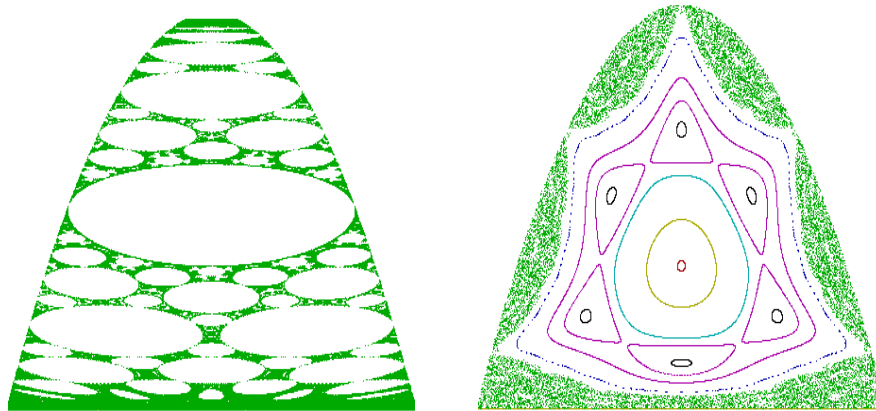


Fig. 13. Poincaré section in velocity space (x, z) for a wedge billiard with wedge half angle $\theta = 44^\circ$ (left) and $\theta = 17^\circ$ (right).

As an example, Fig. 13 shows the velocity space Poincaré sections for $\theta = 44^\circ$ and $\theta = 17^\circ$. One again observes an interesting island and sub-island structure (the islands are generated by stable periodic trajectories) embedded in a more or less extended chaotic sea. With varying wedge angle θ the pattern undergoes interesting structural changes, related to bifurcations of the stability properties of the underlying skeleton of periodic orbits.

More numerical experiments exploring the wedge billiard can be found in H. J. Korsch, H.-J. Jodl: *Chaos – A program collection for the PC* [15]. Let us finally note that also gravitational billiards with a smooth boundary curve have been explored in context with trapping of atoms in gravitational cavities (see, e.g., [16,17]); in particular it has been shown that the parabolic gravitational billiard is integrable.

7 Quantum Billiards

As demonstrated above, billiard systems helped us to investigate and illustrate the fascinating features of chaotic dynamics. However, these systems are classical and, as we all know, on small scales we enter the world of quantum mechanics.

Immediately a seemingly simple question arises: Does chaos also exist for quantum systems? Up to now, this question has not been fully answered. (As a simple exercise, an unexperienced reader should note that quantum dynamics is governed by linear equations, whereas classical chaos originates from nonlinearity.) In a milder formulation, one could pose the question: "Are there signatures of classical chaotic dynamics in quantum systems?" A discussion of this problem can be found in recent textbooks by F. Haake [18] and M. Gutzwiller [19] (see also [20–22]).

Most of our knowledge in this field is again based on computational (and, more recently, also experimental) studies of some model systems. Here we will confine ourselves to quantum studies of billiard systems, or closely related studies of wave dynamics in cavities.

Figure 14 shows an example of such a study of "postmodern quantum mechanics" [21]. Shown is the motion of a wave packet in the stadium billiard [21,23], which is classically ergodic. After a short time the quantum wave function is completely delocalized.

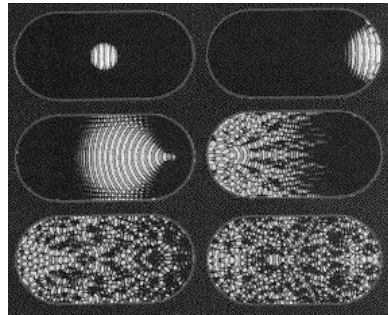


Fig. 14. Motion of an initially localized wavepacket in a stadium billiard [21].

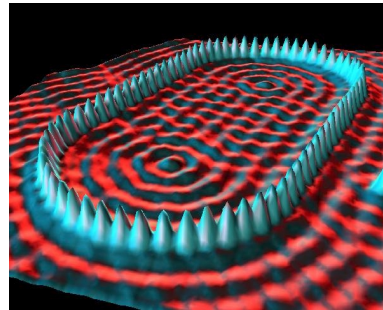


Fig. 15. Quantum corral on a metal surface [24].

Related experimental studies investigate waves on a metal surface and quantum corrals [24], the transport of electrons through billiard shaped quantum dots (see, e.g., [25]) or wave-propagation in various macroscopic systems, which serve as substitute of quantum dynamics because of the similarity of the Helmholtz and the Schrödinger equation. Such systems are microwave cavities (see, e.g., [26–28]), light propagation in optical cavities [29], water surface waves in water tanks [30], or even vibrating soap films [31].

In such studies of quantum (or wave) dynamics the classical chaoticity is manifested in different ways. A prominent example is the nearest-neighbour spacing distribution [19,18], which is Poisson distributed for classically integrable and Wigner distributed for classically ergodic systems. In many cases one also observes so-called 'scars', i.e. states whose wave function localizes on (unstable) classically periodic orbits. It is a topic of contemporary semiclassical analysis to investigate the connection between the classical periodic orbits (note that these

orbits form the skeleton of the classical phase space structure) and the quantum eigenstates [19].

Finally, we would like to mention the recent experiments by M. Raizen investigating the (quantum) dynamics of atoms in strong laser fields, where a gravitational wedge billiard (compare the end of the preceding section) is created by (blue-detuned) laser light which reflects the atoms. The chaotic motion of the atoms is then used in a cooling scheme aiming at the production of a Bose-Einstein condensate [32].

Appendix

Billiard Mapping

Following [9] we give a brief description of the evaluation of the billiard mapping. Let us assume that the angles φ_n and α_n are given. Then the angle ϑ_n between the positive direction of the tangent and the radial ray is given by

$$\tan \vartheta_n = \left. \frac{r(\varphi)}{dr/d\varphi} \right|_n \quad (32)$$

and the direction β_n of the trajectory (i.e. the angle it forms with the $\varphi = 0$ direction) is

$$\beta_n = \pi + \varphi_n + \alpha_n - \vartheta_n. \quad (33)$$

Hence, the straight line trajectory after impact n is given in polar form by

$$R(\varphi) = r(\varphi_n) \frac{\sin(\beta_n - \varphi_n)}{\sin(\beta_n - \varphi)}. \quad (34)$$

The next impact coordinate φ_{n+1} is determined by the intersection of the line (34) with the boundary $r(\varphi)$, i.e. the solution of the equation

$$R(\varphi) - r(\varphi) = 0. \quad (35)$$

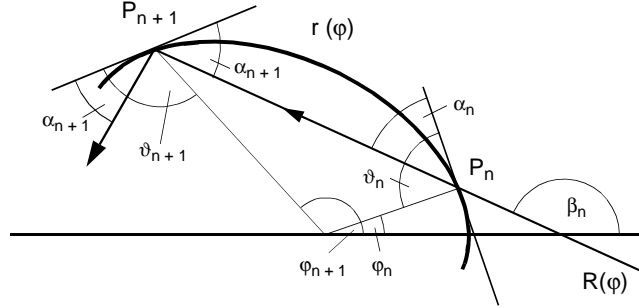


Fig. 16. Billiard mapping $(\alpha_n, \varphi_n) \rightarrow (\alpha_{n+1}, \varphi_{n+1})$.

When $r(\varphi)$ is convex, there exists only one further solution, φ_{n+1} , in addition to φ_n , which is numerically extracted by the Newton iteration scheme. The angle of the trajectory with respect to the tangent in φ_{n+1} is

$$\alpha_{n+1} = \varphi_{n+1} - \varphi_n + \vartheta_n - \vartheta_{n+1} - \alpha_n, \quad (36)$$

as illustrated in Fig. 16. The succeeding boundary reflections are computed by repeating these steps.

Stability Map

For an investigation of the stability properties of an orbit, a useful linearization of the billiard Poincaré mapping $(S_{n+1}, p_{n+1}) \xrightarrow{T} (S_n, p_n)$ and its linearized matrix form

$$\begin{pmatrix} dS_{n+1} \\ dp_{n+1} \end{pmatrix} = \frac{\partial(S_{n+1}, p_{n+1})}{\partial(S_n, p_n)} \begin{pmatrix} dS_n \\ dp_n \end{pmatrix} = \mathbf{M}_{n+1, n} \begin{pmatrix} dS_n \\ dp_n \end{pmatrix} \quad (37)$$

is known [6], which we here formulate for $n = 0$:

$$\mathbf{M}_{1,0} = \begin{pmatrix} -\frac{q_0}{q_1} + \frac{l_{10}}{q_1 \rho_0} & -\frac{l_{10}}{q_0 q_1} \\ -\frac{l_{10}}{\rho_0 \rho_1} + \frac{q_1}{\rho_0} + \frac{q_0}{\rho_1} & -\frac{q_1}{q_0} + \frac{l_{10}}{q_0 \rho_1} \end{pmatrix} \quad (38)$$

with $q_i = \sin \varphi_i$. Here, the length of the straight line segment from P_0 to P_1 is denoted by l_{10} , and ρ_i is the radius of curvature at φ_i given by

$$\rho(\varphi) = \frac{(r^2 + r'^2)^{3/2}}{r^2 + 2r'^2 - rr''}, \quad (39)$$

with $r = r(\varphi)$, $r' = dr/d\varphi$ and $r'' = d^2r/d\varphi^2$. The determinant of \mathbf{M}_{10} is equal to unity, i.e. the mapping T is area-preserving.

The linearization of the iterated map $T^n(S_0, p_0)$ is

$$\mathbf{M}_{n0} = \prod_{i=1}^n \mathbf{M}_{i, i-1}, \quad (40)$$

where the $\mathbf{M}_{i, i-1}$ have the form (38). For the special case of a periodic n -bounce orbit, we have $(S_n, p_n) = (S_0, p_0)$, and the deviation map

$$\mathbf{M}_n = \mathbf{M}_{0, n-1} \mathbf{M}_{n-1, n-2} \cdots \mathbf{M}_{1,0} \quad (41)$$

determines its stability: the eigenvalues of the stability matrix \mathbf{M} are given by

$$\lambda_{\pm} = \frac{1}{2} \left\{ \text{Tr} \mathbf{M} \pm \sqrt{(\text{Tr} \mathbf{M})^2 - 4} \right\} \quad (42)$$

($\det \mathbf{M} = 1$) and therefore the condition for stability is (see, e.g., [15], p.40)

$$|\mathrm{Tr} \mathbf{M}| < 2. \quad (43)$$

In this case the eigenvalues are complex conjugate with modulus unity and small deviations from the fixed point remain small, whereas in the opposite case we have a pair of real valued eigenvalues, where one of them has modulus bigger than one, i.e. a typical deviation from the fixed point will blow up.

Elliptical Billiard: Constant of Motion

It is easy to construct the invariant for the elliptical billiard. Let \mathbf{r}_1 be the vector from the focal point F_1 to the point of impact. Before the collision with the boundary, the angular momentum with respect to F_1 is

$$L_1 = p r_1 \sin \gamma_1, \quad (44)$$

where p is the (constant) momentum and γ_1 is the angle between \mathbf{r}_1 and the trajectory. This angle is determined by the angle α between the trajectory and the tangent and the angle β between the focal ray and the normal at the point of impact by $\gamma_1 = \pi/2 - \alpha - \beta$ (compare Fig. 17). Similarly we have

$$L_2 = p r_2 \sin \gamma_2 \quad (45)$$

with $\gamma_2 = \pi/2 - \alpha + \beta$ (note that the normal bisects the angle between the focal rays).

After the collision with the boundary, we have angular momenta $L_1' = p r_1 \sin \gamma_1'$ and $L_2' = p r_2 \sin \gamma_2'$ with $\gamma_1' = \gamma_2$ and $\gamma_2' = \gamma_1$ as can be seen from Fig. 16. Therefore the product is conserved:

$$L_1' L_2' = L_1 L_2 \quad (46)$$

and elementary algebra yields the formula (18) for the constant of motion $F = L_1 L_2 / p^2$.

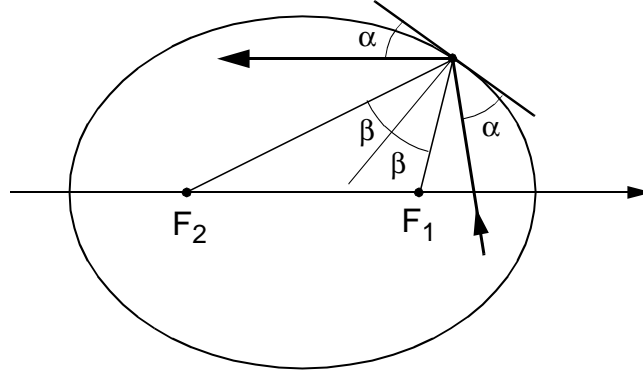


Fig. 17. Billiard mapping $(\alpha_n, \varphi_n) \rightarrow (\alpha_{n+1}, \varphi_{n+1})$.

References

1. A. J. Lichtenberg and M. A. Lieberman, *Regular and Stochastic Motion*, Springer, New York, 1991
2. H. G. Schuster, *Deterministic Chaos*, VCH, Weinheim, 1988
3. M. V. Berry, *Regular and irregular motion*, in S. Jorna, editor, *Topics in Nonlinear Dynamics*, page 16. Am. Inst. Phys. Conf. Proc. Vol. 46, 1978. Reprinted in R. S. MacKay and J. D. Meiss, *Hamiltonian Dynamical Systems*, Adam Hilger, Bristol, 1987
4. M. V. Berry, *Semi-classical mechanics of regular and irregular motion*, in G. Iooss, H. G. Helleman, and R. Stora, editors, *Les-Houches Summer School 1981 on Chaotic Behaviour of Deterministic Systems*, page 171. North-Holland, Amsterdam, 1983
5. V. I. Arnold, *Mathematical Methods of Classical Mechanics*, Springer, New York, 1978
6. M. V. Berry, *Regularity and chaos in classical mechanics, illustrated by three deformations of a circular 'billiard'*, Eur. J. Phys. **2** (1981) 91
7. H. J. Korsch, B. Mirbach, and H.-J. Jodl, *Chaos und Determinismus in der klassischen Dynamik: Billard-Systeme als Modell*, Praxis d. Naturwiss. (Phys.) **36(7)** (1987) 2
8. M. Robnik, *Classical dynamics of a family of billiards with analytic boundaries*, J. Phys. A **16** (1983) 3971
9. H. J. Korsch and H.-J. Jodl, *Chaos - A Program Collection for the PC*, Springer, 1998
10. H. Poritsky, *The billiard ball problem on a table with a convex boundary — An illustrative dynamical problem*, Ann. Math. **51** (1950) 446
11. V. F. Lazutkin, *KAM Theory and Semiclassical Approximations to Eigenfunctions*, Springer, New York, 1991
12. H. E. Lehtihet and B. N. Miller, *Numerical study of a billiard in a gravitational field*, Physica D **21** (1986) 93
13. B. N. Miller and H. Lehtihet, *Chaotic Dynamics: An Instructive Model*, in E.F. Redish and J.S. Risley, editors, *Computers in Physics Instruction*. Addison-Wesley, New York, 1990
14. P. H. Richter, H.-J. Scholz, and A. Wittek, *A breathing chaos*, Nonlinearity **3** (1990) 45
15. H. J. Korsch and H.-J. Jodl, *Chaos - A Program Collection for the PC, 2nd Ed.*, Springer-Verlag, Heidelberg, New-York, 1998
16. H. J. Korsch and J. Lang, *A new integrable gravitational billiard*, J. Phys. A **24** (1990) 45
17. H. Wallis, J. Dalibard, and C. Cohen-Tanoudji, *Trapping atoms in a gravitational cavity*, Appl. Phys. B **54** (1992) 407
18. F. Haake, *Quantum Signatures of Chaos*, Springer, Berlin, Heidelberg, New York, 1992
19. M. C. Gutzwiller, *Chaos in Classical and Quantum Mechanics*, Springer, New York, 1990
20. M. C. Gutzwiller, *Quantum chaos*, Scientific American Jan. (1992) 26, see also www.scitec.auckland.ac.nz/~king/Preprints/book/quantcos/qchao/quantc.htm
21. E. J. Heller and S. Tomsovic, *Postmodern Quantum Mechanics*, Physics Today July (1993) 38, see also <http://www.physics.wsu.edu/Research/tomsovic/chaospage.htm>

22. R. Blümel and W. P. Reinhardt, *Chaos in atomic physics*, Cambridge University Press, Cambridge, 1997
23. S. Tomsovic and E. J. Heller, *Long-time semiclassical dynamics of chaos: The stadium billiard*, Phys. Rev. E **47** (1993) 282
24. M.F. Crommie, C.P. Lut, D.M. Eigler, and E.J. Heller, *Waves on a metal surface and quantum corrals*, Surface Review and Letters **2** (1995) 127, see also <http://www.almaden.ibm.com/vis/stm/corral.html>
25. T. Dittrich, P. Hänggi, G.-L. Ingold, B. Kramer, G. Schön, and W. Zwerger, *Quantum Transport and Dissipation*, Wiley-VCH, Weinheim, 1998
26. H.-D. Gräf, H. L. Harney, H. Lengeler, C. H. Lewenkopf, C. Rangacharyulu, A. Richter, P. Schardt, and H. A. Weidenmüller, *Distribution of eigenmodes in a superconducting billiard with chaotic dynamics*, Phys. Rev. Lett. **69** (1992) 1296
27. J. Stein and H.-J. Stöckmann, *Experimental determination of billiard wave functions*, Phys. Rev. Lett. **68** (1992) 2867
28. A. Richter, *Playing Billiards with Microwaves - Quantum Manifestations of Classical Chaos*, in D.A. Hejhal, J. Friedman, M.C. Gutzwiller, and A.M. Odlyzk, editors, *Emerging Applications of Number Theory, The IMA Volumes in Mathematics and its Applications, Vol. 109*, page 479. Springer, New York, 1999
29. J. U. Nöckel and A. D. Stone, *Ray and wave chaos in asymmetric resonant optical cavities*, Nature **385** (1997) 45
30. R. Blümel, I. H. Davidson, W. P. Reinhardt, H. Lin, and M. Sharnoff, *Quasilinear ridge structure in water waves*, Phys. Rev. Lett. **64** (1990) 241
31. E. Arcos, G. Báez, P. A. Cuatlayol, M. L. H. Prian, and R. A. Méndez-Saldaña, *Vibrating soap films: An analog for quantum chaos on billiards*, Am. J. Phys. **66** (1998) 601
32. M. Raizen and N. Davidson, private communication (2000)